Available online at www.sciencedirect.com
SCIENCE DIRECT®
Journal of Power Sources 122 (2003) 181–187
JOURNAL OF POWER SOURCES
www.elsevier.com/locate/jpowsour

Influence of synthesis conditions on the electrochemical properties of nanostructured amorphous manganese oxide cryogels

Jingsi Yang, Jun John Xu*

Department of Ceramic and Materials Engineering, Rutgers, The State University of New Jersey, Piscataway, NJ 08854, USA

Received 11 February 2003; accepted 28 February 2003

Abstract

Amorphous manganese oxides have received increasing attention in recent years as intercalation cathodes for rechargeable lithium batteries. The sol–gel method is a versatile method for achieving nanostructured amorphous oxides. In this paper, two different sol–gel routes are investigated, where nanostructured amorphous manganese oxide cryogels are obtained via freeze drying Mn(IV) oxide hydrogels formed in situ. In one route the hydrogels are formed by reaction between a solution of sodium permanganate and a solution of disodium fumarate, and in the other route by reaction between a solution of sodium permanganate and solid fumaric acid. Highly homogeneous monolithic manganese oxide hydrogels are obtained from both synthesis routes with precursor concentrations between 0.1 and 0.2 M. The freeze drying method proves to be an efficient method for obtaining nanostructured amorphous manganese oxide cryogels out of the hydrogels. Depending on the synthesis conditions of the hydrogels, the resultant cryogels can yield very high specific capacities for lithium intercalation and excellent rate performance. The cryogel with the best performance exhibits 289 mAh/g at a *C*/100 rate and 174 mAh/g at a 2*C* rate. Strong dependence of electrochemical properties of the cryogels on the synthesis conditions of the parent hydrogels has been observed. The different electrochemical properties are believed to be due to different surface areas and local structures of the cryogels derived from hydrogels synthesized under different conditions. This strong dependence gives rise to the possibility of achieving promising intercalation materials through tailoring the surface area and the local structure of amorphous manganese oxides by adjusting sol–gel synthesis conditions.

Keywords: Li battery; High rate; Sol–gel

1. Introduction

The increasing demand of portable electronic devices and the prospect of electric and hybrid vehicles are driving development of rechargeable lightweight batteries. Rechargeable lithium batteries can store more than twice as much energy per unit weight and volume as other rechargeable systems. Lithium intercalation hosts as the positive electrode (cathode) are vital to the chemistry and the specific energy of these batteries. The high cost and toxicity of the commercially used $LiCoO_2$ have prompted extensive searches for alternatives. Manganese oxides have seen overwhelming interest as inexpensive and environmentally friendly cathode candidates, and manganese oxides and lithium manganese oxides of numerous crystalline structures have been extensively investigated [1–8]. In recent years, manganese oxides of amorphous or nanocrystalline structures have also attracted increasing attention [9–19]. Advantages of these materials include very high lithium intercalation capacity, and in some cases also excellent cycling performance.

Most of these amorphous or nanocrystalline manganese oxides are synthesized via redox synthesis routes in aqueous or non-aqueous solutions to directly yield powders. Compared with these methods, sol–gel synthesis and processing offers an attractive route, one characterized by homogeneous mixing of reactants at the molecular level, more precise control over the composition and morphology of the resulting phases, and convenience for thin film fabrication. The sol–gel approach has been employed for the synthesis of various intercalation compounds. Sol–gel derived vanadium pentoxide (V_2O_5) gels have been extensively investigated as lithium intercalation hosts [20–25]. There have also been a number of reports on sol–gel derived manganese oxides, including birnessite- and hollandite-type manganese oxides and partially crystallized lithiated manganese oxide [26–31]. We recently reported a sol–gel route to a nanostructured amorphous manganese oxide cryogel [32]. The cryogel exhibits very high lithium intercalation capacity and excellent rate capability. These studies demonstrate the advantages of

* Corresponding author. Tel.: +1-732-445-5606; fax: +1-732-445-5595.
E-mail address: johnxu@rci.rutgers.edu (J.J. Xu).

0378-7753/03/$ – see front matter © 2003 Elsevier Science B.V. All rights reserved.
doi:10.1016/S0378-7753(03)00532-9

sol–gel synthesis and processing as a versatile approach for achieving various intercalation oxides of desired properties.

A salient feature of sol–gel derived intercalation compounds appears to be dependence of their structures and properties on synthesis conditions. This might be particularly true for sol–gel derived manganese oxides considering the exceedingly rich structural variety that they may display. It has been reported that crystalline manganese oxides derived from sol–gel routes can have a variety of structures depending on the synthesis route used. The structure of the resulting material is even very sensitive to the precursor concentration as well as the types of ions present in the sol–gel reaction [33–37]. In our recent research, we are concerned with amorphous manganese oxides derived from hydrogels [32]. The manganese oxide hydrogels are transformed into dry gels directly via freeze drying, without any heat treatment. Significant structural relaxation or morphological changes would be unlikely to occur during such a sub-ambient temperature freeze drying process. Therefore, variations in synthesis parameters for the synthesis of the hydrogel might be expected to result in amorphous manganese oxide dry gels with different local structures and morphologies and hence different electrochemical properties. To the best of our knowledge, investigations on the dependence of the local structure and morphology of sol–gel derived amorphous manganese oxides on synthesis conditions have not been reported. Understanding this dependence is of interest to understanding the sol–gel process involved in the synthesis of manganese oxides. At the same time, understanding this dependence would help to lead to materials with superior properties. Considering the greater degree of freedom in composition and local structure for an amorphous phase than for a crystalline phase, even greater opportunity might exist for optimizing properties and performance of an amorphous material through control of its synthesis conditions.

In this paper, manganese oxide hydrogels were synthesized by two different routes and with different precursor concentrations. The freeze drying method was used to obtain manganese oxide cryogels from the hydrogels. Electrochemical properties of the cryogels derived from hydrogels synthesized from the two routes and with different precursor concentrations are characterized. Influence of the hydrogel synthesis conditions on electrochemical properties of the resultant cryogel is analyzed and discussed.

2. Experimental

Manganese oxide hydrogels were prepared by two routes. The first route was by mixing a solution of disodium fumarate with a solution of sodium permanganate. The molar ratio of the two reactants (disodium fumarate:sodium permanganate) was 1:3. The concentration of sodium permanganate after mixing the two solutions was controlled to be 0.10, 0.15 or 0.20 M, respectively. The second route was by mixing solid fumaric acid with a solution of sodium permanganate. The molar ratio of the two reactants (fumaric acid:sodium permanganate) was 1:3. The initial concentration of sodium permanganate was controlled to be 0.10, 0.15 or 0.20 M, respectively. Gellation in all cases occurred and highly homogeneous monolithic hydrogels resulted. The gellation time varied from a few minutes to 1 day, depending on the synthesis route used and the precursor concentration. After rigorous rinsing in deionized water to remove unreacted materials and impurity ions, the hydrogels were frozen inside a glass utensil using liquid nitrogen, and freeze dried under vacuum for 24 h using a Flexi-Dry^{TM} freeze dryer to obtain dry gels called cryogels. The cryogels were named as G1, G2 and G3 for those obtained from the first route, corresponding to the precursor concentration of 0.10, 0.15 and 0.20 M, respectively, and G4, G5 and G6 for those obtained from the second route, corresponding to the precursor concentration of 0.1, 0.15 and 0.20 M, respectively.

Flame atomic absorption (Perkin-Elmer HGA 400) was performed to analyze the composition of the cryogels. A redox titration [38] was performed to determine the mean oxidation state of manganese. Specific surface area was measured from nitrogen physisorption by the Brunauer–Emmett–Teller (BET) method. X-ray powder diffraction was performed with a Siemens Diffraktometer® using Cu Kα radiation, with a 2θ step size of 0.05° and a dwelling time of 10 s at each step. A graphite monochromator was mounted between the sample and the detector to filter noise signals from possible fluorescence induced by the incident X-ray. Morphologies of the cryogels were investigated by Field Emission Scanning Electron Microscopy (FESEM).

For electrochemical characterization, the cryogel materials were stirred with Ketjen black carbon powders and a polytetrafluoroethylene (PTFE) binder in a weight ratio of 60:30:10 (active material:carbon:binder) in cyclohexane overnight. After vacuum drying to remove the cyclohexane, the mixture was rolled, punched and pressed into 1/4 in. diameter pellets with a thickness around 150–200 μm. These pellets were dried at 80 °C under vacuum for 24 h in a vacuum oven that serves as the antechamber of an argon-circulating glovebox. After drying, they were directly transferred into a glovebox without involving any intermediate transfer procedure or exposure to air. They were tested inside the glovebox in laboratory glass cells with lithium metal foils as the counter and reference electrodes and 1 M $LiClO_4$ in 1:1 propylene carbonate:ethylene carbonate as the electrolyte.

3. Results and discussion

Despite the advantages of the sol–gel approach in synthesizing metal oxides, the number of elements whose pure oxides can be obtained in the form of a hydrogel is relatively limited. For most metal oxides, organic segments with hydroxyl groups at the end are required in order for the oxide units to be bonded together through a process

akin to the polymerization process. One could obtain a Mn(IV) oxide gel by gellation of Mn(II) organometallic compounds in aqueous solutions, followed by calcination in air or oxygen to transform the Mn(II) oxide to a Mn(IV) oxide [39,40]. The calcination process usually leads to well-crystallized structures. The process for synthesizing Mn(IV) oxide hydrogels by reducing permanganate salts with organic reducing agents is a so-called in situ process [33], which involves many chemical steps. First Mn(VII) is reduced to Mn(IV). Then the Mn(IV) ions experience hydration and hydrolysis processes to form aquo-hydroxo complexes $[Mn(OH)_h(OH_2)_{N-h}]^{(4-h)+}$, where the number N is the coordination number of the Mn(IV) ion in solution, which is normally six, namely, octahedral coordination, and the number h presents the ratio of hydrolysis which is controlled by many factors such as the concentration of the ions and the aciditiy of the solution. Condensation of these Mn(IV) octahedral units through olation or oxolation may occur simultaneously to generate polycations, which can be regarded as Mn(IV) oxide clusters. Finally a sol-to-gel transition occurs when these manganese oxide clusters are cross-linked by organic fragments resulting from partial oxidization of the organic reducing agent [33,34,37]. The reducing agent used for this process is normally an organic compound, and organic segments resulting from partial oxidization of the organic compound are believed to play an important role in cross-linking the Mn(IV) oxide units. In the present study, disodium fumarate and fumaric acid are used as the reducing agent in the two synthesis routes, respectively.

For the permanganate to Mn(IV) oxide hydrogel process, the precursor concentration is a crucial factor for successfully obtaining a highly homogeneous monolithic hydrogel. With both synthesis routes in our study, it has been found that when the precursor concentration is less than 0.1 M, only a flocculent gel can be achieved instead of a monolithic one, most likely due to the deficiency of the concentration of linking segments. With increase of the precursor concentration, gellation becomes easier and occurs sooner and faster. When the precursor concentration is too high, the reaction rate becomes too fast to control, and it is difficult to let the reaction proceed uniformly throughout the solution to result in a highly homogeneous hydrogel. The gel easily loses homogeneity or even direct precipitation of powders may occur. In our experiments with both synthesis routes, highly homogeneous monolithic hydrogels were obtained when the precursor concentration was between 0.1 and 0.2 M.

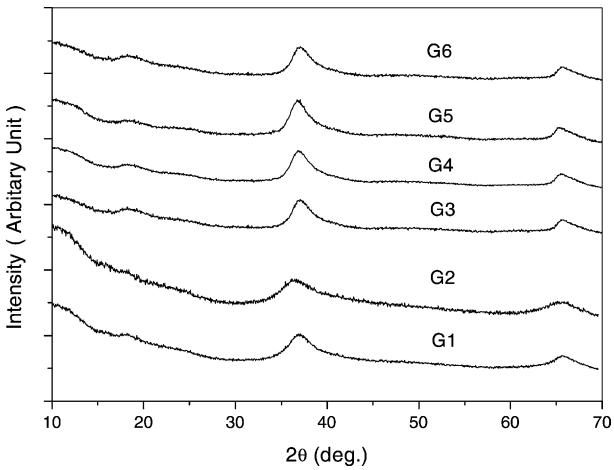

Fig. 1. XRD patterns of amorphous manganese oxide cryogels.

The freeze drying method was used to remove water in the manganese oxide hydrogels. At the sub-ambient temperature of the freeze drying process, the amorphous nature of the oxide phase in the hydrogel was preserved. For all the cryogels obtained from freeze drying the hydrogels, X-ray powder diffraction patterns, Fig. 1, show their structure is largely amorphous and lacks long range order. At the same time, since the freeze drying process only involved sublimation from ice to vapor and the high surface tension associated with the liquid–vapor interface was avoided, the porous structure of the oxide phase inherent in the hydrogel may be largely preserved [32]. The BET surface areas of cryogels obtained from freeze drying hydrogels synthesized by the second route, namely, samples G3, G4 and G5, are all above 300 m^2/g (Table 1), which are very high values for manganese oxides.

The chemical composition of the cryogels were determined by using a combination of elemental analysis by atomic absorption and determination of the mean oxidation state of manganese by a redox titration [38]. Elemental analysis revealed the weight percentage of manganese and

Table 1
Synthesis conditions and chemical compositions of amorphous manganese oxide cryogels

	Reaction	Precursor concentration (M)	Mean oxidation state of Mn	Formula	Unidentified mass		Surface area (m^2/g)
					Weight per mole (g/mol)	Weight fraction (wt.%)	
G1	$NaMnO_4 + C_4H_2O_4Na_2$	0.10	3.93	$Na_{0.29}MnO_{2.11}$	10.5	9.9	52
G2		0.15	3.86	$Na_{0.28}MnO_{2.07}$	10.8	10.2	36
G3		0.20	3.76	$Na_{0.24}MnO_{2.00}$	9.9	9.6	44
G4	$NaMnO_4 + C_4H_4O_4$	0.10	3.61	$Na_{0.28}MnO_{1.95}$	8.1	8.0	302
G5		0.15	3.88	$Na_{0.28}MnO_{2.13}$	14.4	13.1	352
G6		0.20	3.74	$Na_{0.20}MnO_{1.97}$	7.2	7.3	356

sodium in the material and indirectly yielded the molecular weight of the sample. The amount of the oxygen anion in the sample was determined based on the mean oxidation state of manganese and the concentration of Na^+. The remaining weight, ca. 7–13 wt.%, is unidentified mass. It most likely consists of organic residues resulting from partial oxidation of the organic reducing agent as discussed before [33,34,37], and structure water. Structure water is usually present in manganese oxides synthesized from low temperature aqueous routes [26,27,29,34]. The molecular formula thus obtained, the mean oxidation state of Mn and the amount of the unidentified mass, along with BET surface areas of the cryogel samples, are listed in Table 1.

From Table 1, the chemical compositions of all the cryogel samples are fairly close to each other. The mean oxidation state of Mn in all the samples is close to 4+, and the amount of sodium ions in all the samples is similar. The amount of unidentified mass attributed to organic residues and structural water in all the samples is more or less the same too. However, the electrochemical properties of these samples are quite different from each other. Fig. 2 shows plots of specific capacity for lithium intercalation versus cycle number for the cryogels. The cryogels were first discharged from the open-circuit voltage (OCV) (3.4 V) to 1.5 V versus Li^+/Li, and subsequently cycled between 4.0 and 1.5 V, at a *C*/5 discharge/charge rate, which corresponds to a current density of ca. 1 mA/cm^2. For the samples obtained from freeze drying hydrogels synthesized by the first route, namely, samples G1, G2 and G3, initial specific capacities of 45, 52 and 103 mAh/g are obtained, respectively. For the samples obtained from freeze drying hydrogels synthesized by the second route, namely, samples G4, G5 and G6, initial specific capacities of 87, 143 and 217 mAh/g are obtained, respectively. Therefore, a great difference in specific capacity is observed between the samples obtained from the two different synthesis routes. At the same time, a strong dependence of specific capacity on the precursor concentration is observed. For both synthesis routes, the higher the precursor concentration, the higher the specific capacity of the resultant cryogel. Considering the similar chemical compositions and mean oxidation states of manganese in all the samples, such great dependence of electrochemical properties on the synthesis conditions cannot be explained on the basis of the small differences in chemical composition and mean oxidation state of Mn of the resultant cryogels.

It appears that the large difference in specific capacities between the samples obtained from the first synthesis route (G1, G2 and G3) and those from the second route (G4, G5 and G6) may be explained by the large difference in specific surface areas resulting from the different synthesis routes. The specific surface areas for samples G1, G2 and G3 are a few tens of m^2/g, while they are above 300 m^2/g for G4, G5 and G6. Under the investigation of FESEM, these cryogels show a porous microscopy characterized by a bicontinuous network consisting of a solid phase and pores. The solid phase is the active material which lithium ions diffuse into and out of during the intercalation/deintercalation processes. The large difference in specific surface areas between samples G1, G2, G3, and samples G4, G5, G6 directly translates into a large difference in the characteristic thickness of the solid phase and hence in the diffusion length for the lithium intercalation reaction. It is widely accepted that solid-state diffusion inside the active material is usually the rate-limiting step for intercalation reactions. As diffusion time is inversely proportional to the square of diffusion length, a significant difference in diffusion length would lead to an even more pronounced difference in intercalation capacity at a given current rate. This factor is likely largely responsible for the marked difference in specific capacities between the cryogels obtained from the two different synthesis routes. The large difference in specific surface area between these two groups of samples are in turn likely due to the different reaction rates in the two synthesis routes. For the first route, where the reaction is between a solution of sodium permanganate and a solution of disodium fumarate, the mixing of two solutions leads to instant mixing of

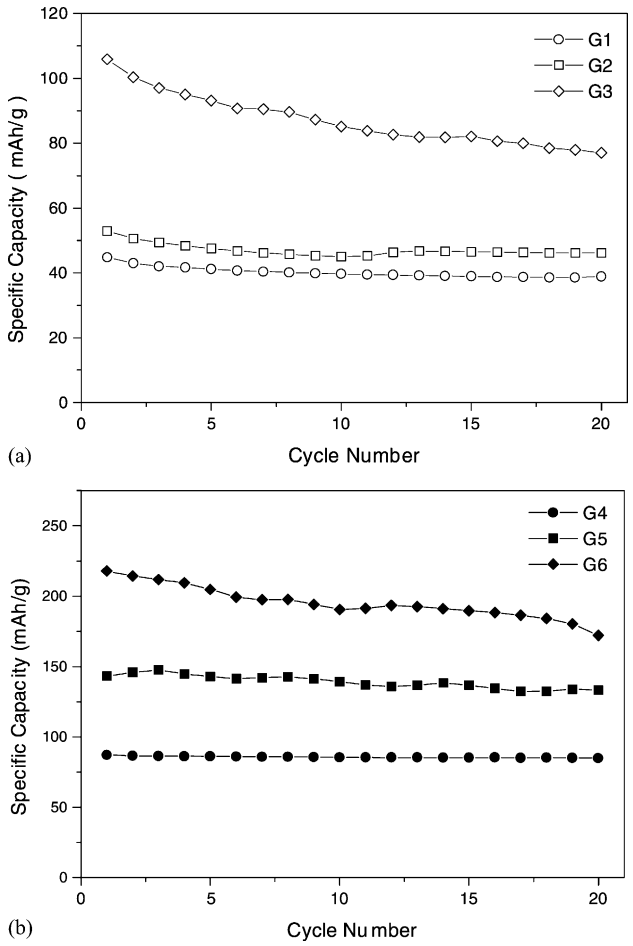

Fig. 2. Plots of specific capacity vs. cycle number of amorphous manganese oxide cryogels obtained from hydrogels synthesized by (a) reaction between a solution of sodium permanganate and a solution of disodium fumarate; (b) reaction between a solution of sodium permanganate and solid fumaric acid. Rate: *C*/5.

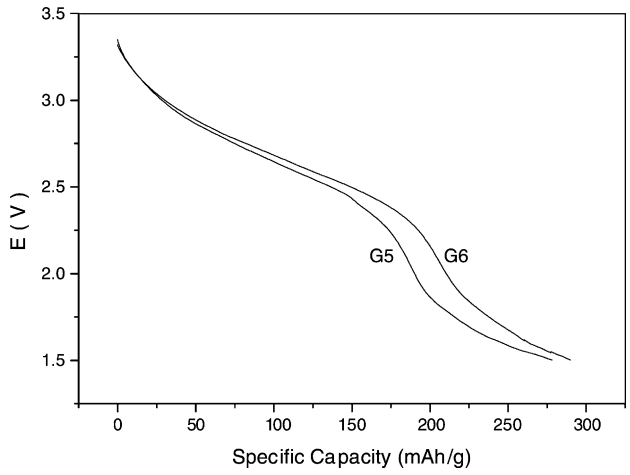

Fig. 3. Discharge profiles of samples G5 and G6 at *C*/100 rate.

reactants at a molecular level. The rate for reduction, hydrolysis and condensation mostly likely is much greater than that in the second route, where a solution of sodium permanganate is mixed with solid fumaric acid powders. The difference in reaction rate is readily supported by experimental observations that the gellation time in the first route is much shorter than that in the second route at the same precursor concentration. With the much higher reaction rate in the first route, it is most likely that much larger polycations or manganese(IV) oxide clusters are formed before they are cross-linked together by the organic segments to form the hydrogel. Therefore, thick solid phase and low surface areas of the resultant cryogels would be expected.

As seen from Fig. 2, the capacity of the amorphous manganese oxide cryogels also shows a strong dependence on the precursor concentration used in synthesis of the parent hydrogel. Samples G5 and G6 are studied in detail in order to understand the origin of this dependence. Fig. 3 shows the discharge curves of G5 and G6 at a very slow rate of *C*/100. The two curves are close to each other and the specific capacities exhibited by the two samples are very similar. Since kinetic factors are most likely insignificant at this very slow rate, it can be concluded that the intrinsic intercalation capacity or the number of intercalation sites is similar for the two samples. Therefore, the significant difference in specific capacities at the high rate of *C*/5 (Fig. 2) must be due to kinetic factors. Considering that both samples have the same surface area of ca. 350 m^2/g, the possibility of the effect of different thickness of the solid phase or diffusion length may also be largely ruled out. Therefore, the difference in intercalation capacity at the *C*/5 rate appears likely to be due to a difference in intrinsic kinetic properties. To verify this point, chemical diffusion coefficients of Li ions, D_{Li}, in both samples were determined by the GITT method, as described in [41]. The D_{Li} is calculated by:

$$\tilde{D} = \frac{4}{\pi}\left(\frac{V_M}{SFZ_i}\right)^2\left[I_0\frac{dE/d\delta}{dE/d\sqrt{t}}\right]^2 \quad (1)$$

The symbols in the equation have their usual meaning as in [41]. Under identical testing conditions and using the apparent surface area of the testing electrode for the surface area *S* in the equation, the D_{Li} values of both G5 and G6 samples are calculated to be on the order of magnitude of 10^{-10} cm^2/s. However, the D_{Li} value for the G6 sample is two times that for the G5 sample. In the GITT method, a parameter that is difficult to determine and that may cause severe errors is the surface area *S* used in the equation. The surface area that should be used for the accurate determination of the diffusion coefficient is probably somewhere between the internal surface area of the composite electrode and the apparent surface area of the electrode. However, this is not a critical factor here since we are primarily interested in the relative magnitudes of the diffusion coefficients in the two samples. Both samples as the active material have the same specific surface area, and composite electrodes based on the two samples were fabricated under identical conditions. Therefore, the conclusion, reached under identical testing conditions, that the lithium ion diffusion coefficient in the G6 sample is two times that in the G5 sample, is valid.

The two times difference in diffusion coefficient would lead to significant differences in intercalation capacities in tests where the rate of intercalation is limited by lithium diffusion inside the active material, which is usually the case unless the current rate used is extremely low. From Fick's law, the diffusion depth of the diffusing species is proportional to the square root of the diffusion coefficient. A two times difference in diffusion coefficient would translate to a ca. 40% difference in diffusion depth, and hence a ca. 40% difference in intercalation capacity at a given period of time. Moreover, the discharging and charging tests were done between a fixed voltage range (between 4.0 and 1.5 V versus Li^+/Li). The lower the diffusion coefficient, the faster the lithium ions become saturated at the surface of the active material during discharge, and depleted during charge, namely, the faster the sample reaches the voltage limits. Therefore, the time allowed for intercalation within a given voltage range is shorter for the sample that has a lower diffusion coefficient than for the sample that has a higher diffusion coefficient. These two effects combined would result in a difference of even greater than 40% in intercalation capacities at current rates where lithium diffusion inside the active material is the rate-limiting step. In fact, the difference in initial intercalation capacity between samples G5 and G6 is 50%, in fair agreement with the theoretical analysis.

It appears likely that the difference in intrinsic kinetic properties of these amorphous cryogels is due to difference in their local structures, which in turn is induced by their different synthesis conditions. In the work of Ching and Suib [34,35], the structure of materials obtained from calcining gels derived from reducing potassium permanganate by glucose or fumaric acid showed a strong dependence on the precursor concentration used in the synthesis of the gel. This dependence was explained by the different concentrations of potassium ions in these crystallized materials. In our case,

the concentrations of sodium ions are very close to each other and the structures shown by X-ray powder diffraction (Fig. 1) are also difficult to distinguish from each other due to their amorphous nature. From the XRD patterns, diffuse peaks around 18, 36 and 65° suggest that there exists some level of short- and intermediate-range order. As proposed by Salmon [42], although amorphous materials such as glasses cannot be described as nanocrystalline, crystal structures can be useful tools for understanding and manipulation of disordered materials at intermediate scales. In our case, this kind of short- and intermediate-range order and the way the Mn(IV) octahedra are linked together to form an ordered local structure can have a significant dependence on the synthesis conditions, considering the hydrolysis and condensation processes that occurred during the synthesis. As mentioned before, Mn(IV) ions, which are normally octahedrally coordinated, exist in forms of aquo-hydroxo complexes $[Mn(OH)_h(OH_2)_{N-h}]^{(4-h)+}$. The Mn(IV) octahedral are piled up to form manganese oxide clusters through an olation or oxolation process, and the way they pile up is influenced by the hydrolysis ratio of the cation. In general, one, two or three oxo or hydroxo ligands can be formed between two Mn(IV) octahedra, which give rise to corner-, edge- and face-sharing octahedra in the final structure, respectively [43]. Since the hydrolysis ratio is a function of the precursor concentration, the way these octahedra are linked together would likely show a dependence on the precursor concentration. Therefore, it is reasonable to expect that hydrogels synthesized at different precursor concentrations have different local structures. When transforming from the hydrogel to the cryogel, the freeze drying method at subambient temperature should preserve those local structures, for there is not sufficient thermal energy to activate rearrangement or relaxation of the structures. In the work of Le Goff et al., properties of layered manganese dioxides synthesized from precipitation and sol–gel routes are proposed to be strongly dependent on the stacking of the layers and the nature of the host site [28]. In our case, difference in local structures may have similar effect on properties of the amorphous materials, such as the mobility of lithium ions during diffusion, which gives rise to different lithium intercalation capacities at a given discharge/charge rate. However, it is very difficult to reveal the difference in local structure of the amorphous materials from the X-ray powder diffraction patterns. It is a challenge to determine the local structure of the amorphous materials, and this challenge must be met in future research using more advanced structural characterization techniques.

Among all the cryogel samples, sample G6 exhibits the highest specific capacity and excellent rate performance. Fig. 4 shows the specific capacity of sample G6 as a function of discharge rate. The material exhibits 289, 217 and 174 mAh/g at *C*/100, *C*/5 and 2*C* rates, respectively. These are very high reversible specific capacities for a manganese oxide, in comparison with, for example, the specific capacity of ca. 125 mAh/g for the spinel $LiMn_2O_4$. A specific capacity of 174 mAh/g at a 2*C* rate (6.9 mA/cm^2) demonstrates the excellent rate capability of the material. To the best of our knowledge, it is the highest reversible specific capacity reported for a manganese oxide at such a high rate, although the voltage range used is wide, from 3.4 to 1.5 V versus Li^+/Li. Further investigations, in light of the dependence of electrochemical properties on the synthesis conditions, might lead to materials of even better properties. Such dependence of electrochemical properties on synthesis conditions would be generally true for the synthesis of kinetically rather than thermodynamically stable materials, such as the amorphous cryogels in the present study, and would give rise to possibilities for tailoring electrochemical properties through control of sol–gel synthesis conditions.

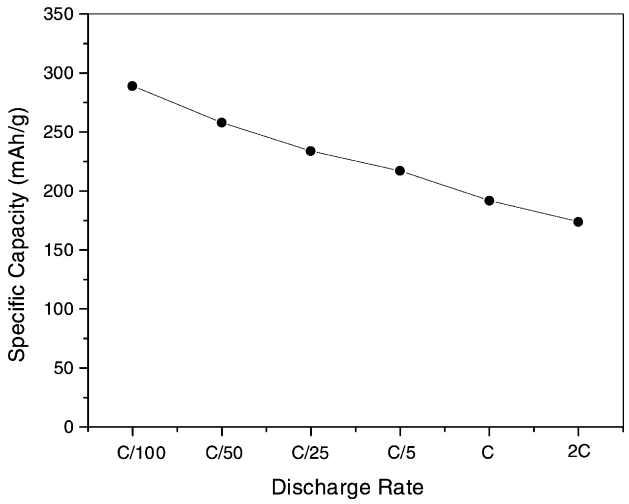

Fig. 4. Specific capacity vs. rate of sample G6.

4. Conclusion

Manganese oxide hydrogels were synthesized by two different sol–gel routes. The first was by reaction between a solution of sodium permanganate and a solution of disodium fumarate, and the second by reaction between a solution of sodium permanganate and solid fumaric acid. Highly homogeneous monolithic hydrogels were obtained from both synthesis routes in the precursor concentration range between 0.1 and 0.2 M. The freeze drying method was used to extract water from the hydrogels and amorphous manganese oxide cryogels resulted. The electrochemical properties of the cryogel show strong dependence on both the synthesis route and the precursor concentration used for the synthesis of the parent hydrogel. Cryogels obtained from hydrogels synthesized by the second route exhibit much higher specific capacities for lithium intercalation than those obtained from hydrogels synthesized by the first route. For both routes, the higher the precursor concentration used for the synthesis of the hydrogel, the higher the specific capacity of the resultant cryogel. It appears that these differences in electrochemical properties are caused by differences in the specific surface

area and local structure of the cryogels, which in turn are influenced by the synthesis route or the precursor concentration used for the synthesis of the parent hydrogels. The cryogel with the best electrochemical properties exhibit lithium intercalation capacities of 289, 217 and 174 mAh/g at *C*/100, *C*/5 and 2*C* rates, respectively. The dependence of electrochemical properties on synthesis conditions would give rise to possibilities of achieving intercalation materials of desired properties through control of sol–gel synthesis conditions.

Acknowledgements

Financial support from a Workforce Excellence grant of the New Jersey Commission on Higher Education is gratefully acknowledged.

References

[1] M.M. Thackeray, W.I.F. David, P.G. Bruce, J.B. Goodenough, Mater. Res. Bull. 18 (1983) 461.
[2] M.M. Thackeray, J.O. Thomas, M.S. Whittingham, Mater. Res. Bull. 25 (2000) 39.
[3] M.S. Whittingham, P.Y. Zavalij, Solid State Ionics 131 (2000) 109.
[4] G. Cedar, A. Van der Ven, M.K. Aydinol, JOM 50 (1998) 35.
[5] B. Scrosati, Electrochim. Acta 45 (2000) 2461.
[6] T. Eriksson, T. Gustafsson, J.O. Thomas, Electrochem. Solid State Lett. 5 (2002) A35.
[7] J.M. Tarascon, D. Guyomard, Electrochim. Acta 38 (1993) 1221.
[8] A.R. Armstrong, P.G. Bruce, Nature 381 (1996) 499.
[9] J.J. Xu, A.J. kinser, B.B. Owens, W.H. Smyrl, Electrochem. Solid State Lett. 1 (1998) 1.
[10] J.J. Xu, G. Jain, J. Yang, Electrochem. Solid State Lett. 5 (2002) A152.
[11] J.J. Xu, J. Yang, G. Jain, Electrochem. Solid State Lett. 5 (2002) A223.
[12] J. Kim, Manthiram, Nature 390 (1997) 265.
[13] J. Kim, A. Manthiram, Electrochem. Solid State Lett. 2 (1999) 55.
[14] D. Im, A. Manthiram, J. Electrochem. Soc. 149 (2002) A1001.
[15] F. Leroux, L.F. Nazar, Solid State Ionics 100 (1997) 103.
[16] A.I. Palos, M. Anne, P. Strobel, Solid State Ionics 138 (2001) 203.
[17] S. Kang, J.B. Goodenough, L.K. Rabenberg, Electrochem. Solid State Lett. 4 (2001) A49.
[18] P. Lucas, C.A. Angell, J. Electrochem. Soc. 147 (2000) 4459.
[19] G.J. Moore, R. Portal, A. Le Gal La Salle, D. Guyomard, J. Power Sources 97–98 (2001) 393.
[20] B.B. Owens, S. Passerini, W.H. Smyrl, Electrochim. Acta 45 (1999) 215.
[21] B.B. Owens, W.H. Smyrl, J.J. Xu, J. Power Sources 81–82 (1999) 150.
[22] S. Passerini, J.J. Ressler, D.B. Le, B.B. Owens, W.H. Smyrl, Electrochim. Acta 44 (1999) 2209.
[23] F. Zhang, S. Passerini, B.B. Owens, W.H. Smyrl, Electrochem. Solid State Lett. 4 (2001) A221.
[24] D.B. Le, S. Passerini, J. Guo, J. Ressler, B.B. Owens, W.H. Smyrl, J. Electrochem. Soc. 143 (1996) 2099.
[25] W. Dong, D.R. Rollison, B. Dunn, Electrochem. Solid State Lett. 3 (2000) 457.
[26] S. Franger, S. Bach, J.P. Pereira-Ramos, N. Baffier, J. Electrochem. Soc. 147 (2000) 3226.
[27] S. Franger, S. Bach, J. Farch, J.P. Pereira-Ramos, N. Baffier, J. Power Sources 109 (2002) 262.
[28] P. Le Goff, N. Baffier, S. Bach, J.P. Pereira-Ramos, J. Mater. Chem. 4 (1994) 875.
[29] J.W. Long, K.E. Swider-Lyons, R.M. Stroud, D.R. Rolison, Electrochem. Solid State Lett. 3 (2000) 453.
[30] J.W. Long, R.M. Stroud, D.R. Rolison, J. Non-Cryst. Solids 285 (2001) 288.
[31] S. Passerini, F. Coustier, M. Giorgetti, W.H. Smyrl, Electrochem. Solid State Lett. 2 (1999) 483.
[32] J.J. Xu, J. Yang, Electrochem. Commun., in press.
[33] S. Bach, M. Henry, N. Baffier, J. Livage, J. Solid State Chem. 88 (1990) 325.
[34] S. Ching, S.L. Suib, Inorg. Chem. 19 (1997) 263 (Comments).
[35] S. Ching, J.L. Roark, N. Duan, S.L. Suib, Chem. Mater. 9 (1997) 750.
[36] S. Ching, D.J. Petrovay, M.L. Jorgensen, S.L. Suib, Inorg. Chem. 36 (1997) 883.
[37] S. Ching, E.J. Welch, S.M. Hughes, A.B.F. Bahadoor, S.L. Suib, Chem. Mater. 14 (2002) 1292.
[38] M.J. Katz, R.C. Clarke, W.F. Nye, Anal. Chem. 28 (1956) 507.
[39] Y. Lee, Y. Sun, K. Nahm, Solid State Ionics 109 (1998) 285.
[40] S.H. Park, K.S. Park, S.S. Moon, Y.K. Sun, K.S. Nahm, J. Power Sources 92 (2001) 244.
[41] W. Weppner, R.A. Huggins, J. Electrochem. Soc. 124 (1977) 1569.
[42] P.S. Salmon, Nature Materials 1 (2002) 87.
[43] J. Jolivet, M. Henry, J. Livage, E. Bescher, Metal Oxide Chemistry and Synthesis, Wiley, New York, 2000.